AIP Advances

Zero Poynting vector $\mathbf{E} \| \mathbf{H}$ Beltrami field cylindrical cavity resonators

Cite as: AIP Advances **12**, 075314 (2022); https://doi.org/10.1063/5.0100710
Submitted: 30 May 2022 • Accepted: 25 June 2022 • Published Online: 15 July 2022

Ryo Mochizuki, Naoki Shinohara and Atsushi Sanada

Zero Poynting vector E ∥ H Beltrami field cylindrical cavity resonators

Cite as: AIP Advances 12, 075314 (2022); doi: 10.1063/5.0100710
Submitted: 30 May 2022 • Accepted: 25 June 2022 •
Published Online: 15 July 2022

Ryo Mochizuki,[1,a] Naoki Shinohara,[1] and Atsushi Sanada[2]

AFFILIATIONS

[1] Research Institute for Sustainable Humanosphere, Kyoto University, Uji, Kyoto 611-0011, Japan
[2] Graduate School of Engineering Science, Osaka University, Toyonaka, Osaka 560-8531, Japan

[a] Author to whom correspondence should be addressed: ryo_mochizuki@rish.kyoto-u.ac.jp

ABSTRACT

In this paper, we present novel cylindrical cavity resonators accommodating spatially and temporally zero Poynting vector Beltrami standing waves with the parallel electric and magnetic fields ($\mathbf{E} \parallel \mathbf{H}$). We introduce the special boundary conditions, i.e., longitudinal electromagnetic conductor (LEMC) on which zero longitudinal electromagnetic components are enforced and circumferential electromagnetic conductor (CEMC) on which zero circumference electromagnetic components are enforced in an axisymmetric waveguide system, and show that the zero Poynting vector $\mathbf{E} \parallel \mathbf{H}$ Beltrami standing wave is generated as a superposition of dual degenerated axisymmetric TM and TE standing waves in a cylindrical resonator using the LEMC and CEMC boundary conditions. We present physical implementation methods of the LEMC and CEMC boundary conditions composed of the circumferentially arranged corrugations and the concentrically aligned cylindrical thin fins, respectively. In addition, we numerically demonstrate the Beltrami standing field generation and reveal its peculiar electromagnetic properties: the spatially and temporally $\mathbf{E} \parallel \mathbf{H}$ with zero Poynting vector distribution, identical electric and magnetic energy density distributions, and zero local reactive energy flow.

I. INTRODUCTION

Propagation modes in a waveguide are determined by boundary conditions. For instance, the circular waveguide used in high-frequency circuits/systems supports TM and TE modes with the boundary condition $E_\phi = E_z = 0$ on the sidewall.[1] Let us consider a singular axisymmetric waveguide with the special anisotropic boundary condition of zero longitudinal electric and magnetic components, $E_z = 0$ and $H_z = 0$, on the sidewall, i.e., strictly speaking, a lateral equidistance surface from the axis. What kind of propagation modes can exist in the waveguide? Although the boundary condition is apparently impractical, it is artificially achievable with a structured surface discussed in the following. In the following, we refer to the boundary condition as a longitudinal electromagnetic conductor (LEMC).

Applying the LEMC boundary condition on $\rho = a$ to Maxwell's equations, we obtain a set of orthogonal axisymmetric TM and TE solutions in the cylindrical coordinate system as follows:

TM mode:

$$\mathbf{E} = E_0\left[-\mathrm{i}\frac{\beta}{k_c}J_1(k_c\rho)\mathbf{e}_\rho + J_0(k_c\rho)\mathbf{e}_z\right]\mathrm{e}^{\mathrm{i}(\beta z-\omega t)}, \tag{1}$$

$$\mathbf{H} = -\mathrm{i}\frac{E_0}{\eta_0}\frac{k_0}{k_c}J_1(k_c\rho)\mathbf{e}_\phi\mathrm{e}^{\mathrm{i}(\beta z-\omega t)}; \tag{2}$$

TE mode:

$$\mathbf{E} = E_0\frac{k_0}{k_c}J_1(k_c\rho)\mathbf{e}_\phi\mathrm{e}^{\mathrm{i}(\beta z-\omega t)}, \tag{3}$$

$$\mathbf{H} = -\mathrm{i}\frac{E_0}{\eta_0}\left[-\mathrm{i}\frac{\beta}{k_c}J_1(k_c\rho)\mathbf{e}_\rho + J_0(k_c\rho)\mathbf{e}_z\right]\mathrm{e}^{\mathrm{i}(\beta z-\omega t)}, \tag{4}$$

where J_n is the nth Bessel function of the first kind, k_0 is the wavenumber in free space, β is the propagation constant, k_c is the

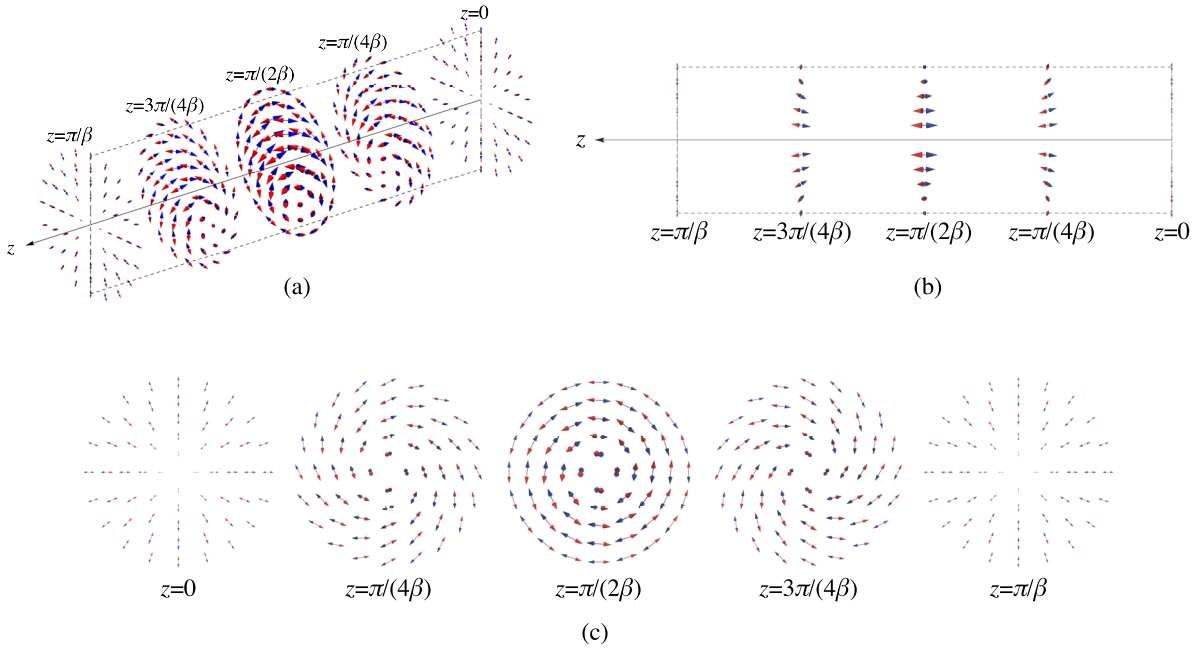

FIG. 1. Beltrami field distribution on five cross sections within a half wavelength. (a) General view. (b) On the cross section including the z axis. (c) On the five cross sections with $z = m\pi/(4\beta)$, where $m = 0, 1, 2, 3$, and 4. The red and blue arrows correspond to the **E** and **H** fields, respectively. The electric and magnetic fields are parallel to each other. Note that the arrows are perfectly axisymmetric though they seem to be asymmetric in (a) due to the matter of a perspective.

cut-off wavenumber, $\eta_0 = \sqrt{\mu_0/\varepsilon_0}$ is the intrinsic impedance of free space, and i is the imaginary unit. It is noted that **E** and **H** are interchangeable between the TM and TE modes, i.e., Eqs. (1) and (2) are in the same form with Eqs. (3) and (4), respectively. It is also noted that these TM and TE modes degenerate with the identical cut-off wavenumber p_{01}/a, where p_{01} is the first zero of J_0.

Let us consider a superposition of the standing waves of these TM and TE modes with the phase shift of $\pm\pi/2$ in both the time and longitudinal position. The total electromagnetic field in the waveguide is represented by

$$\mathbf{E} = \mathrm{e}^{-\mathrm{i}\omega t} E_0 \left[\frac{\beta}{k_\mathrm{c}} J_1(k_\mathrm{c}\rho)\sin(\beta z)\mathbf{e}_\rho \pm \frac{k_0}{k_\mathrm{c}} J_1(k_\mathrm{c}\rho)\cos(\beta z)\mathbf{e}_\phi + J_0(k_\mathrm{c}\rho)\cos(\beta z)\mathbf{e}_z \right], \tag{5}$$

$$\mathbf{H} = -\mathrm{i}\mathrm{e}^{-\mathrm{i}\omega t} \frac{E_0}{\eta_0} \left[\frac{\beta}{k_\mathrm{c}} J_1(k_\mathrm{c}\rho)\sin(\beta z)\mathbf{e}_\rho \pm \frac{k_0}{k_\mathrm{c}} J_1(k_\mathrm{c}\rho)\cos(\beta z)\mathbf{e}_\phi + J_0(k_\mathrm{c}\rho)\cos(\beta z)\mathbf{e}_z \right]. \tag{6}$$

Equations (5) and (6) suggest that the electric and magnetic fields are parallel to each other, $\mathbf{E} \parallel \mathbf{H}$, and thus, the Poynting vector vanishes everywhere. The electromagnetic standing wave is classified as a new type of Beltrami fields.[2–16] Figure 1 shows a typical electromagnetic field distribution of the Beltrami field. It is clearly seen that the electric and magnetic fields are parallel to each other everywhere despite the fact that they are neither TM, TE, nor TEM and have a complicated distribution with longitudinal components.

The boundary conditions providing the phase shifts of $\pm\pi/2$ for the Beltrami field are given by the peculiar conditions $E_\phi = 0$ and $H_\phi = 0$ on both ends of the waveguide. In the following, we refer to the boundary condition as a circumferential electromagnetic conductor (CEMC). The CEMC is also artificially achievable, which will be discussed in Sec. II.

II. REALIZATION OF LEMC AND CEMC

Here, we consider realization methods of the LEMC and CEMC. A waveguide with the LEMC boundary condition, $E_z = 0$ and $H_z = 0$, on the lateral sidewall can be implemented with the circumferentially arranged fine corrugations compared with the wavelength. The cross section of the waveguide is shown in Fig. 2(a). The corrugation is characterized by the corrugation depth d_LEMC and the spacing between the adjacent corrugations s_LEMC. The spacing s_LEMC is to be selected sufficiently smaller than the free-space wavelength λ_0 ($s_\mathrm{LEMC} \ll \lambda_0$). The corrugation enforces $E_z = 0$ at $\rho = a$, which implies that the waveguide supports a TM_{01} mode with the cut-off wavenumber $k_\mathrm{c}^\mathrm{TM} = p_{01}/a$. Note that the cut-off wavenumber is dependent only on a, not on d_LEMC, and operates as a circular waveguide with the radius a. The propagation constant for the TM_{01} mode, β^TM, is determined by $(\beta^\mathrm{TM})^2 = {k_0}^2 - (k_\mathrm{c}^\mathrm{TM})^2$. As for the TE mode, the corrugated sidewall operates as a short-ended stub with the length d_LEMC. The LEMC boundary condition at $\rho = a$ is realized by appropriately choosing the length $d_\mathrm{LEMC} = \pi a/(2p_{01})$

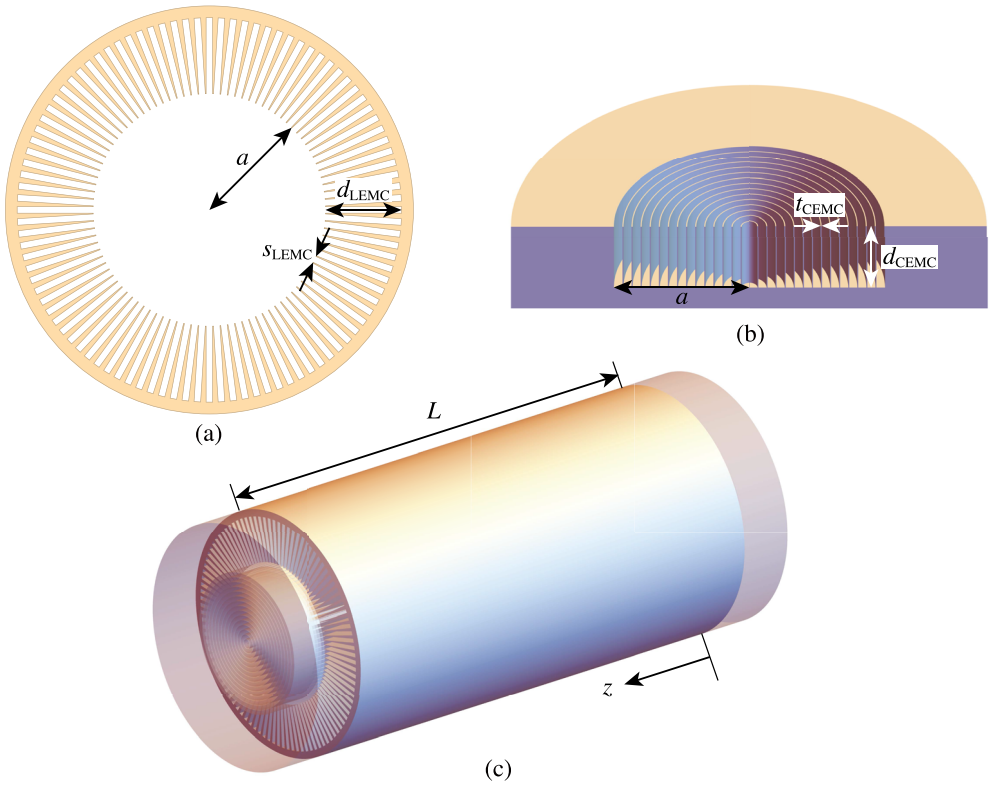

FIG. 2. Physical implementations of (a) the LEMC, (b) the CEMC, and (c) the **E** ∥ **H** cavity resonator. a is the inner radius, d_{LEMC} is the corrugation depth, and s_{LEMC} is the interval between the adjacent corrugations in the LEMC. t_{CEMC} is the fin thickness, and d_{CEMC} is the fin depth in the CEMC. L is the resonator length (the length of the LEMC region or the interval between the CEMC ends).

(see the Appendix). It is noteworthy that the LEMC boundary condition is maintained regardless of the frequency with the cut-off wavenumber k_c^{TE} identical to that of the TM_{01} mode, k_c^{TM}. The propagation constant for the TE mode is determined by $(\beta^{TE})^2 = k_0^2 - (k_c^{TE})^2$, which is also identical to that of the TM_{01} mode, β^{TM}, leading to the fact that the dispersion relations of the TM_{01} and TE modes in the waveguide agree with each other. Incidentally, the depth d_{LEMC} has to be slightly longer than $\pi a/(2p_{01})$ due to the fringing effect. The effect can be taken into account by full-wave simulations.

The CEMC boundary condition, $E_\phi = 0$ and $H_\phi = 0$, at both ends can also be implemented with the concentric cylindrical thin fins shown in Fig. 2(b). The fins reflect the TE mode with the reflection coefficient of −1 on the top surface, whereas they reflect the TM mode with the reflection coefficient of $e^{ik_0 d_{CEMC}}$. Therefore, the CEMC is realized by choosing the depth $d_{CEMC} = \pi/(2k_0)$. It is noted that the CEMC operation is frequency dependent. It is also noted that the fringing effect is taken into account to determine d_{CEMC}.

The Beltrami cavity resonator with **E** ∥ **H** can be composed by a combination of the LEMC and CEMC boundaries as shown in Fig. 2(c), which will be discussed in Sec. III.

III. BELTRAMI CAVITY RESONATOR

A. Design

We demonstrate the **E** ∥ **H** Beltrami resonator operation with the presented LEMC and CEMC implementations. Suppose that the lateral LEMC boundary is implemented with 100ϕ-segments of corrugation with the duty ratio of 0.1, and we let the resonator length L be 30 mm. Now, we determine the radius a and the corrugation depth d_{LEMC} consistently so that the TM and TE dispersion relations coincide with each other by using a commercial full-wave simulator Ansys HFSS (High Frequency Structure Simulator). Figure 3 shows a unit circumferential sector for the calculations. Applying the periodic boundary conditions to the ρ–z planes, we calculate the dispersion characteristics for both the TM_{01} and TE modes. Here, we assume the conductivity of the resonator material is 5.8×10^8 S/m (corresponding to copper). We optimize a and d_{LEMC} so that the cut-off frequencies for the TM_{01} and TE modes coincide with each other by considering the fact that the cut-off frequency of the TM_{01} mode is determined by a, whereas that of the TE mode is determined by d_{LEMC}. The optimized parameters are a = 13.26 mm and d_{LEMC} = 8.851 mm, which leads to the cut-off frequency of 8.57 GHz. According to the dispersion characteristics, the resonant frequency

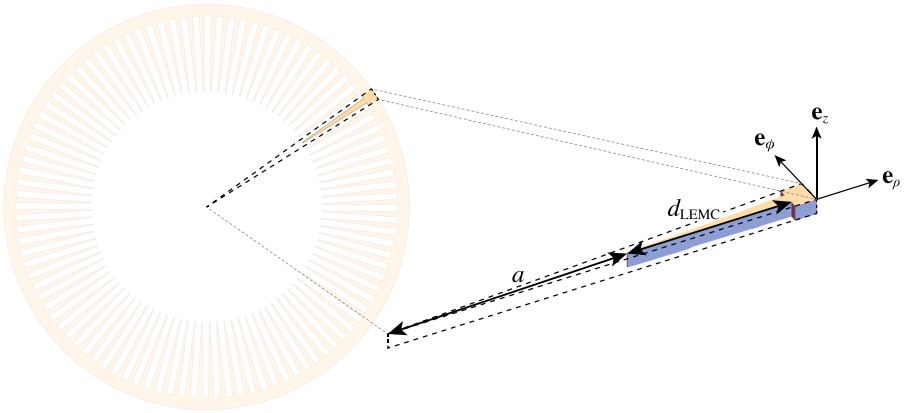

FIG. 3. A circumferential sector of the LEMC waveguide for the TM and TE mode dispersion relation calculations. The periodic boundary condition is applied to the ρ–z planes of the sector.

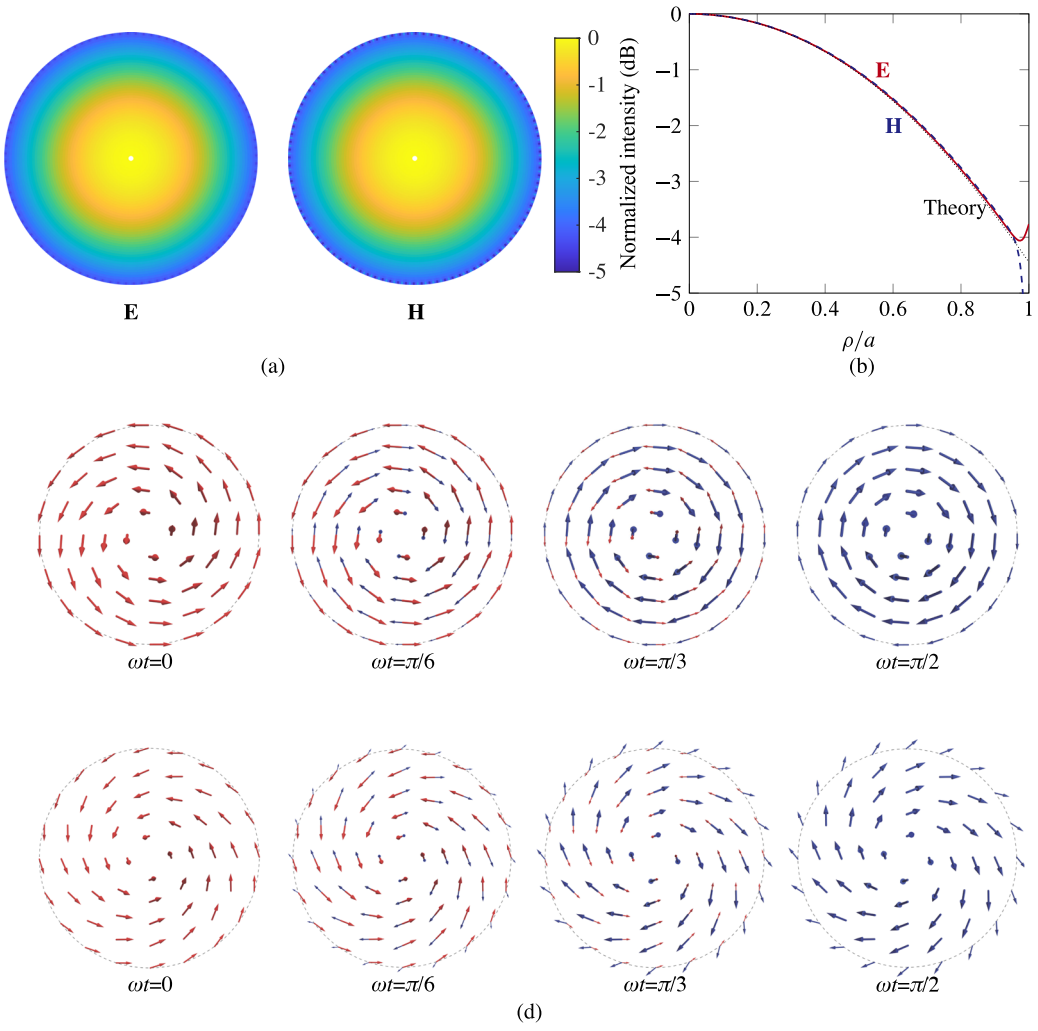

FIG. 4. The simulated field profiles of the designed resonator. (a) The field intensities of **E** and **H** at the center transverse section of $z = L/2$. The intensities are normalized by the maximum value on the axis $\rho = 0$. (b) The z-dependencies of the normalized intensities of **E** and **H**. The red solid and blue dashed lines correspond to **E** and **H**, respectively. The dotted line corresponds to the theoretical curve derived from Eqs. (5) and (6). The time series snapshots of the field distributions of **E** and **H** at the center transverse sections of (c) $z = L/2$ and (d) $z = L/4$. The red and blue arrows correspond to **E** and **H**, respectively. The dashed circle depicts the periphery of the waveguide region, $\rho = a$.

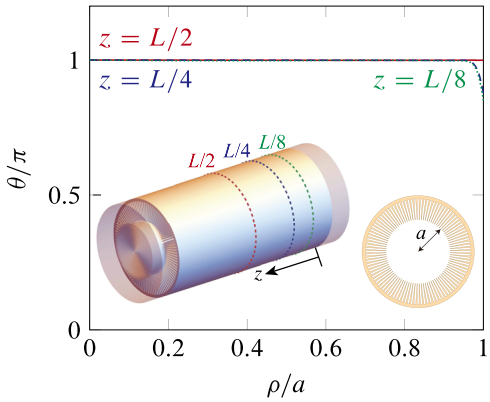

FIG. 5. The z-dependency of the angle θ between **E** and **H**. The red solid, blue dashed, and green dotted lines correspond to θ on the transverse cross sections of $z = L/2$, $L/4$, and $L/8$, respectively.

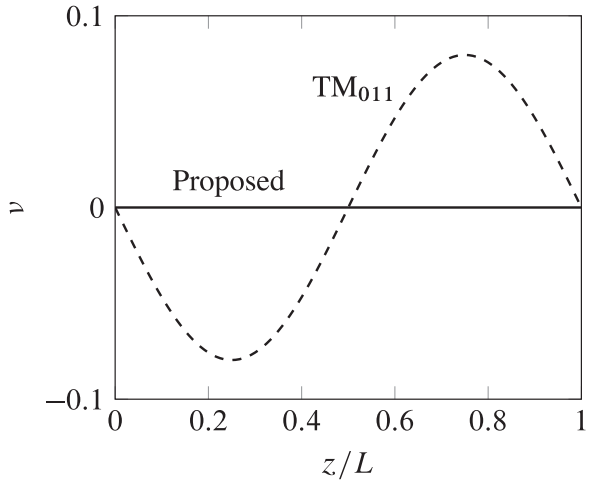

FIG. 7. The z-dependency of the reactive energy flow normalized by the stored energy. The solid and dashed lines correspond to those in the proposed resonator and in a convention TM_{011} resonator, respectively.

of the first mode with $\beta^{TM}L = \beta^{TE}L = \pi$ is 9.91 GHz. As for the CEMC boundary, suppose that the CEMC is composed of 15 equally spaced cylindrical fins with the thickness $t_{CEMC} = 0.1$ mm$(0.0017\lambda_g)$ as shown in Fig. 2(b). The corrugation depth d_{CEMC} is numerically determined as 7.605 mm by taking into account the fringing effect at the resonant frequency of 9.91 GHz.

B. Fields, energy distributions, and Poynting vectors

Figures 4(a) and 4(b) show the simulated electromagnetic field intensities on the central transverse section at $z = L/2$ and those along the radial direction with the theoretical prediction, respectively. The field intensities are normalized by their maximum values at $\rho = 0$. It is noted that both the simulated electric and magnetic field distributions exhibit the identical Besselian distribution as the theoretical prediction except in the vicinity of the periphery of the waveguide. Figures 4(c) and 4(d) show the time series snapshots of the simulated electromagnetic fields on the two transverse sections at $z = L/2$ and $L/4$, respectively. It is seen from these figures that the electric and magnetic fields are parallel to each other regardless of the z-position at any time, leading to temporally zero Poynting vector. Incidentally, the non-parallel electric and magnetic fields in the vicinity of the LEMC boundary are due to the fringing effect.

Figure 5 shows the simulated angle distributions between electric and magnetic fields, θ (except **E** = 0 or **H** = 0), as a function of the position ρ. It is quantitatively confirmed from the figure that the electric and magnetic fields are parallel except in the periphery of the waveguide. It is noted that the electric and magnetic fields are completely parallel at the center $z = L/2$ due to the geometrical symmetry.

Now, we consider the time-averaged electric and magnetic energy density on the transverse cross section, u_e and u_m, given by

$$u_e(z) = \frac{\varepsilon_0}{4}\int_0^{2\pi}\int_0^a \mathbf{E}\cdot\mathbf{E}^*\rho d\rho d\phi, \tag{7}$$

$$u_m(z) = \frac{\mu_0}{4}\int_0^{2\pi}\int_0^a \mathbf{H}\cdot\mathbf{H}^*\rho d\rho d\phi. \tag{8}$$

Figure 6(a) shows the simulated z-dependencies of u_e and u_m in the designed resonator. For comparison, Fig. 6(b) shows the theoretical z-dependencies of u_e and u_m for a conventional short-circuited TM_{011} resonator with the same radius a and length L. It is noted from these figures that the proposed resonator exhibits peculiar u_e and

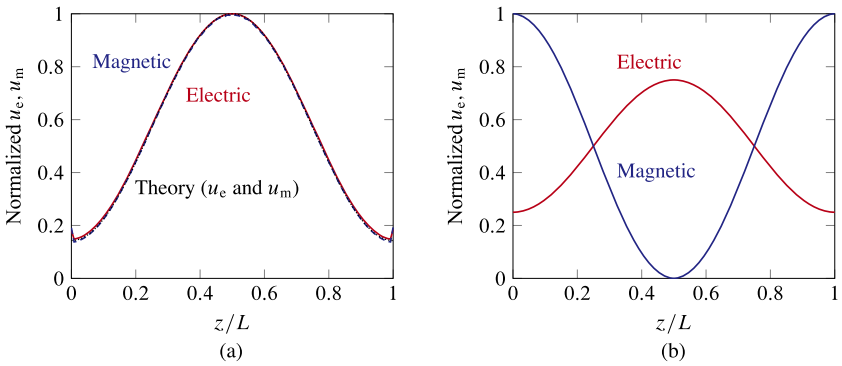

FIG. 6. The z-dependencies of the surface integrals of the electric and magnetic energy densities over the transverse section, u_e and u_m, normalized by the maximum magnetic energy density value. (a) In the proposed resonator. The red solid and blue dashed lines correspond to u_e and u_m, respectively. The black dotted line corresponds to the theoretical curve. (b) In a conventional TM_{011} cylindrical cavity. The red and blue lines correspond to u_e and u_m, respectively.

u_m distributions with the same z-dependency except in the vicinity of each end as opposed to the fact that the conventional TM_{011} resonator has different u_e and u_m distributions with their peaks in the different positions. Incidentally, the integrals of u_e and u_m are identical.

Figure 7 shows the z-dependency of the reactive energy flow passing through the cross section in a quarter of the period, $\pi/2\omega$, normalized by the total stored energy, i.e.,

$$v(z) = \frac{\frac{1}{\omega}\mathrm{Im}\left\{\int_0^{2\pi}\int_0^a \frac{1}{2}\left(\mathbf{E}\times\mathbf{H}^*\right)\cdot\mathbf{e}_z\rho\mathrm{d}\rho\mathrm{d}\phi\right\}}{\int_0^L (u_e+u_m)\mathrm{d}z}. \tag{9}$$

In the proposed resonator, v becomes zero almost everywhere due to the parallel electromagnetic field nature as opposed to the fact that v becomes non-zero in the conventional resonator due to the non-local energy exchange between electric and magnetic fields.

IV. CONCLUSIONS

In this paper, we have presented the zero Poynting vector $\mathbf{E} \parallel \mathbf{H}$ Beltrami field cylindrical cavity resonators. We have shown that a cylindrical waveguide with the LEMC boundary condition supports dual degenerated axisymmetric TM and TE propagation modes and that a superposition of the standing waves of the TM and TE modes leads to an $\mathbf{E} \parallel \mathbf{H}$ Beltrami field with a certain TM and TE phase shift of $\pm\pi/2$ in both the time and longitudinal position. We have also shown that the phase shift can be realized by the CEMC. In addition, we have proposed concrete feasible structures of the LEMC and CEMC, i.e., the circumferentially arranged corrugation and the concentrically aligned cylindrical thin fins, respectively. Moreover, we have numerically demonstrated an $\mathbf{E} \parallel \mathbf{H}$ resonator operation at 9.91 GHz by designing the LEMC with 100 corrugations and the CEMC with 15 fins and confirmed its unusual electromagnetic properties of (1) the parallel electric and magnetic fields with temporally zero Poynting vector distribution, (2) the agreement of the electric and magnetic energy density distributions, and (3) zero local reactive energy flow. A potential application exploiting the peculiar $\mathbf{E} \parallel \mathbf{H}$ Beltrami field is a novel closed microwave cavity resonator for Lorentz-force-free plasma heating and acceleration.

ACKNOWLEDGMENTS

This work was supported by JSPS KAKENHI Grant No. JP20J14118.

AUTHOR DECLARATIONS

Conflict of Interest

The authors have no conflicts to disclose.

Author Contributions

Ryo Mochizuki: Conceptualization (lead); Data curation (lead); Formal analysis (lead); Investigation (lead); Methodology (lead); Validation (equal); Visualization (equal); Writing – original draft (lead); Writing – review & editing (equal). **Naoki Shinohara:** Conceptualization (supporting); Data curation (supporting); Formal analysis (supporting); Investigation (supporting); Methodology (supporting); Project administration (equal); Resources (lead); Supervision (equal); Validation (equal); Writing – original draft (supporting); Writing – review & editing (equal). **Atsushi Sanada:** Conceptualization (supporting); Data curation (supporting); Formal analysis (supporting); Investigation (supporting); Methodology (supporting); Project administration (equal); Supervision (equal); Validation (equal); Visualization (equal); Writing – original draft (supporting); Writing – review & editing (equal).

DATA AVAILABILITY

The data that support the findings of this study are available within the article.

APPENDIX: PROOF OF THE LEMC BOUNDARY CONDITION REALIZATION WITH $d_{LEMC} = \pi a/(2p_{01})$

Consider propagating waves in the corrugation region, $a \le \rho \le a + d_{LEMC}$. Their electromagnetic fields are represented by

$$\begin{aligned} E_\phi &= \frac{k_0}{k_\rho}E_{cor}\,\sin(k_\rho(\rho-a-d_{LEMC}))\mathrm{e}^{\mathrm{i}(k_z z-\omega t)},\\ H_\rho &= -\frac{k_z}{k_\rho}\frac{E_{cor}}{\eta_0}\sin(k_\rho(\rho-a-d_{LEMC}))\mathrm{e}^{\mathrm{i}(k_z z-\omega t)},\\ H_z &= -\mathrm{i}\frac{E_{cor}}{\eta_0}\cos(k_\rho(\rho-a-d_{LEMC}))\mathrm{e}^{\mathrm{i}(k_z z-\omega t)}, \end{aligned} \tag{A1}$$

where E_{cor} is a coefficient, and k_ρ and k_z are the ρ- and z-components of the wavevector, respectively. On the other hand, the electromagnetic fields outside the corrugation region, $\rho \le a$, are represented by

$$\begin{aligned} E_\phi &= \frac{k_0}{k_c^{TE}}E_0 J_1\left(k_c^{TE}\rho\right)\mathrm{e}^{\mathrm{i}(\beta z-\omega t)},\\ H_\rho &= -\frac{\beta}{k_c^{TE}}\frac{E_0}{\eta_0}J_1\left(k_c^{TE}\rho\right)\mathrm{e}^{\mathrm{i}(\beta z-\omega t)},\\ H_z &= -\mathrm{i}\frac{E_0}{\eta_0}J_0\left(k_c^{TE}\rho\right)\mathrm{e}^{\mathrm{i}(\beta z-\omega t)}, \end{aligned} \tag{A2}$$

where E_0 is a coefficient, and β^{TE} and k_c^{TE} are the phase constant and cut-off wavenumber of the TE mode of Eqs. (3) and (4), respectively. The field continuity on the interface, $\rho = a$, requires the transcendental equation $\cos(k_c^{TE}d_{LEMC})J_1(k_c^{TE}a) + \sin(k_c^{TE}d_{LEMC})J_0(k_c^{TE}a) = 0$. By solving the equation with $d_{LEMC} = \pi a/(2p_{01})$, we obtain $k_c^{TE} = p_{01}/a$ as the lowest order solution, and therefore, $k_c^{TE}d_{LEMC} = \pi/2$. By substituting $k_c^{TE}d_{LEMC} = \pi/2$ at $\rho = a$ into (A1), we readily obtain $H_z = 0$ at $\rho = a$. With $E_z = 0$, the LEMC boundary condition is realized at $\rho = a$.

REFERENCES

[1] D. Pozar, *Microwave Engineering*, 4th ed. (Wiley, 2011).
[2] A. Lakhtakia, "Time-dependent Beltrami fields in material continua: The Beltrami-Maxwell postulates," Int. J. Infrared Millimeter Waves **15**, 369–394 (1994).

[3]W. S. Weiglhofer and A. Lakhtakia, "Time-dependent Beltrami fields in free space: Dyadic green functions and radiation potentials," Phys. Rev. E **49**, 5722–5725 (1994).
[4]A. Lakhtakia, *Beltrami Fields in Chiral Media* (World Scientific, 1994).
[5]C. Chu and T. Ohkawa, "Transverse electromagnetic waves with $\vec{E} \parallel \vec{B}$," Phys. Rev. Lett. **48**, 837–838 (1982).
[6]K. K. Lee, "Comments on "Transverse electromagnetic waves with $\vec{E} \parallel \vec{B}$"," Phys. Rev. Lett. **50**, 138 (1983).
[7]C. Chu, "Chu responds," Phys. Rev. Lett. **50**, 139 (1983).
[8]H. Zaghloul, K. Volk, and H. A. Buckmaster, "Comment on "Transverse electromagnetic waves with E‖B"," Phys. Rev. Lett. **58**, 423 (1987).
[9]C. Chu and T. Ohkawa, "Chu and Ohkawa respond," Phys. Rev. Lett. **58**, 424 (1987).
[10]A. Khare and T. Pradhan, "Transverse electromagnetic waves with finite energy, action, and $\int \vec{E} \cdot \vec{B} d^4x$," Phys. Rev. Lett. **49**, 1227–1228 (1982).
[11]F. C. Michel, "Transverse electromagnetic waves with nonzero $\vec{E} \cdot \vec{B}$," Phys. Rev. Lett. **52**, 1351 (1984).
[12]H. Zaghloul and H. A. Buckmaster, "Transverse electromagnetic standing waves with E‖B," Am. J. Phys. **56**, 801–806 (1988).
[13]K. Shimoda, T. Kawai, and K. Uehara, "Electromagnetic plane waves with parallel electric and magnetic fields E‖H in free space," Am. J. Phys. **58**, 394–396 (1990).
[14]K. Uehara, T. Kawai, and K. Shimoda, "Non-transverse electromagnetic waves with parallel electric and magnetic fields," J. Phys. Soc. Jpn. **58**, 3570–3575 (1989).
[15]T. Nishiyama, "General plane or spherical electromagnetic waves with electric and magnetic fields parallel to each other," Wave Motion **54**, 58–65 (2015).
[16]R. Mochizuki, N. Shinohara, and A. Sanada, "Time-harmonic electromagnetic fields with E‖B represented by superposing two counter-propagating beltrami fields," Prog. Electromagn. Res. M **104**, 171–184 (2021).